Building Simulation 2003

Eighth International IBPSA Conference
Eindhoven, Netherlands
August 11-14, 2003

CLIMATE AS A PRE-DESIGN TOOL

Darren Robinson
BDSP Partnership
27 Sale Place, London, W2 1YR, UK.

ABSTRACT

This paper describes a new software application for analysing climate data. It is argued that the produced graphical charts can be useful concept stage design tools in their own right. In describing the software this paper presents a review of climate analysis techniques. It is hoped that this review will be of use to the architectural science student. By way of demonstration climatic charts for Limburg, which is close to the conference venue of Eindhoven, are presented. Finally, scope for further development of the software tool is outlined.

INTRODUCTION

Enormous quantities of meteorological data are now available for myriad locations and some excellent programs now exist for deriving hourly data from databases of monthly means. The Swiss program Meteonorm is an excellent case in point (though this paper does not necessarily advocate the use of Meteonorm data for building simulation). However, few tools exist which capitalise on the potential for this data to inform concept design solutions. This paper describes a new design tool that has been developed to fill this niche. ClimPro (short for climate processor) reads in hourly climate data (global and diffuse horizontal solar irradiance, air temperature, relative humidity and wind speed and direction) and, with the global co-ordinates specified, produces a series of graphical design aids relating to solar, daylight, synoptic and ground parameters. Some useful statistics are also produced.

By using output from stochastic modelling climatological databases, climate for practically any location can be easily and swiftly processed. The graphical output from this tool can be used to inform strategic thinking in relation to overheating risk and the potential for different forms of passive cooling, the scope for passive and active heating, the need for and type of shading devices, the extent of glazing for good daylighting and the viability of different renewable energy systems. Some of the output can also be useful later in the design process, for example to optimise shading devices and determine the viability of using photoresponsive lighting controls.

The code that computes the data to produce these charts is written in VB. For convenience Microsoft Excel is used as a host application so that effort is centred upon producing useful output rather than in reproducing a basic graphical capability.

SOLAR AND DAYLIGHTING PARAMETERS

Within this category ClimPro produces sunpath diagrams, daylight availability curves, irradiation surface plots, solar radiation frequency distributions and monthly statistical summaries. Note that examples from the application of ClimPro that follow are based upon an hourly climate file produced by Meteonorm using a monthly means from a 30 year World Meteorological Organisation (WMO) dataset.

Stereographic sunpath diagram

From elementary solar geometry solar altitude (γ) at a given time and location can be determined from the expression:

$$\sin g = \sin i \sin d - \cos i \cos d \cos w \qquad \ldots[1]$$

in which i is the site latitude, w is the solar hour angle and d the solar declination angle is derived from the following Fourier series (after Spencer, 1971):

$$d = 0.006918 - 0.399912\cos t + 0.070257\sin t - 0.006758\cos 2t + 0.000907\sin 2t - 0.002697\cos 3t + 0.00148\sin 3t \qquad \ldots[2]$$

where for the jth day, t is $2p(j-1)/365$.

Since we know that at sunrise the solar altitude is zero, we can rearrange [1] to determine the sunrise hour angle (w'):

$$\cos w' = -\tan i \tan d \qquad \ldots[3]$$

from which the corresponding sunrise or sunset time is $12 \pm 12w'/p$. The remaining solar angular co-ordinate, its azimuth (a), is found from:

$$\cos a = -\sin i \sin g + \sin d / \cos i \cos g \; ; w < p \ldots [4]$$

If $w > p$ (i.e. we are beyond solar noon) then $a = 2p - a$. (where w may be w' for the boundaries of the solar day). Now, the two angular co-ordinates g and a can be translated into planar x, y co-ordinates for plotting on a conventional chart, whereby $x = (p/2 - g)\sin a$ and $y = (p/2 - g)\cos a$. This then places the zenith at the centre of a diagram in which x and y axes extend between $\pm p/2$, so representing a sky vault in stereographic projection. Discretising the solar trajectory to sunset at hourly intervals for the jth day, the associated angular co-ordinates are found from [1] – [4] in which $w = pt/12$. Connecting these points with a curve (e.g. a smoothed scatter plot line using Excel) completes the definition of a sunpath line. To add structure to the diagram it is useful to define sunpaths at say monthly intervals between the winter and summer solstices ($d \approx \pm 23.45\pi/180 \approx \pm 0.4093$). Curves between these two extremes, following solar symmetry, also then apply to the months between the summer and winter solstices. In repeating the above steps (and ignoring perturbations in the earth's rate of rotation as represented by the equation of time) for the set of seven months we can archive in memory the solar co-ordinates that were calculated at the same time (while $g > 0$). Connecting these points (after conversion to planar co-ordinates) creates a set of constant time lines.

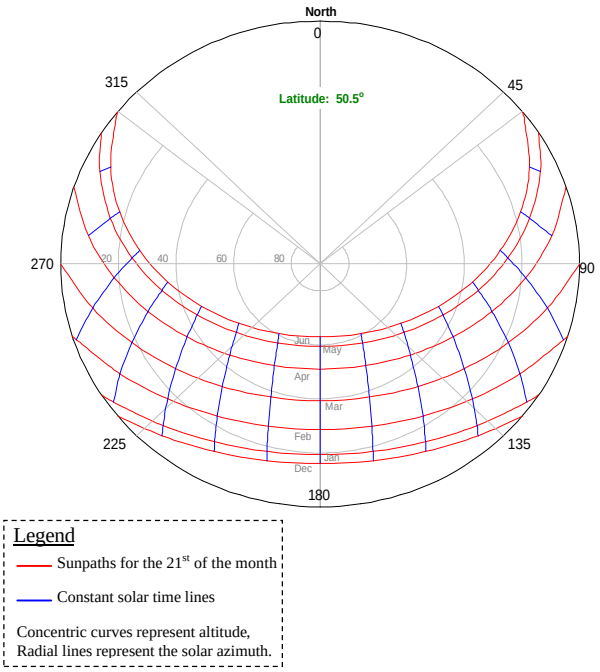

Figure 1 Sunpath diagram for Limburg

To further aid with interpretation it is helpful to define lines of constant solar altitude. These are simply concentric circles in which the radius is a given altitude (say $180g/p$ = 20, 40…80), the azimuth is varied ($0 \rightarrow 2\pi$) and both are translated to planar co-ordinates. With some annotation, and by creating some constant azimuth curves (the inverse of the above process) we can create a sunpath diagram for Limburg (Figure 1). It may be useful to add to this diagram additional *shading protractor* curves that define solar cut-off angles for vertical / horizontal shading devices. Vertical devices may be represented simply by lines of constant azimuth, say at 10° intervals in the range $a_w \pm p/2$ for a wall of azimuth a_w. For horizontal devices an effective altitude is required: $g^* = \tan^{-1}\left(\tan g \cdot \cos|a_w - a|\right)$ with x, y found in the usual way: $(x = (p/2 - g^*)\sin a_w, y = (p/2 - g^*)\cos a_w)$.

Daylight availability curve

Since to derive illuminance we must process time-series solar radiation data, it is important to know the time convention that was used to prepare and archive the data. An hour-centred time convention is typically used. That is for noon the irradiation (J) is integrated from the centre of the preceding hour to that of the following hour (11:30 → 12:30) and divided by time to give irradiance (W), so that it is appropriate to base solar geometry calculations on the hour. Other conventions include hour ending (11:00 → 12:00, the data archived at 12:00) and hour beginning (11:00 → 12:00, data archived at 11:00). In these cases solar calculations are performed on the half-hour (11:30) and this is the case when processing data from Meteonorm, which uses an hour ending time convention. Finally, climate data tends to be archived in local time. As such this data needs to be translated from local (t) to solar (t') time, to determine the appropriate solar angular co-ordinates in the solar processing calculations. To do this we need to correct for displacement from the meridian at which local time is based to that of the site ($?L$), for variations in the Earth's rate of rotation due to the elipticity of the earth's orbit around the sun as well as the earth's tilt as expressed by the equation of time (e) and possibly for daylight savings (d):

$$t' = t + 4\Delta L + e + d \qquad \ldots(5)$$

The equation of time e in [5] is found from the Fourier series after Spencer (1971):

$$e = 229.2\left(\begin{matrix}0.00008 + 0.00187\cos t - 0.0321\sin t - \\ 0.0146\cos 2t - 0.0409\sin 2t\end{matrix}\right) \ldots [6]$$

in which t is as defined in [2] above.

With the sun and the climate data synchronised, diffuse (or indeed global) horizontal illuminance (E_d) can be derived from hourly irradiance using the luminous efficacy model due to Perez (Perez 1990):

$$E_d = I_d\left(A_1 + A_2 w + A_3 \sin g + A_4 \ln \Delta\right) \quad \ldots[7]$$

where A_1 to A_4 are coefficients (Table 1) that depend on sky clearness (e):

$$e = \frac{I_g / I_d + 1.041 Z^3}{1 + Z^3} \quad \ldots[8]$$

for which Z is the solar zenith angle ($p/2$ - g). w in [7] represents atmospheric precipitable water content, cm (which may be set to 2 with little loss in accuracy) and the sky brightness Δ is found thus:

$$\Delta = I_d / I_o \sin g \quad \ldots[9]$$

where sin$g$ represent the number of optical air masses that the solar radiation passes through and I_o is the extraterrestrial horizontal irradiance ($I_o = G(1 + 0.033\cos[360\,jp/365 \cdot 180])$ in which G is the solar constant - 1367 Wm^{-2} and the term in brackets corrects for elipticity of the solar orbit). All that remains is to accrue counts to the jth daylight bin, defined by a given bin width i, so that $j = int(I_d/i)$.

By charting the cumulative external horizontal illuminance distribution (Figure 2) it is possible, given a room daylight factor, to approximately determine the number of hours during the year that a given threshold external illuminance (E') is exceeded – say due to photoreponsive switching ($E' = E_{in} / \left(10^{-2} \cdot DF\right)$); read up until this intersects the curve and long to the y-axis to find the number of hours that lights could be switched off).

For example, if we have (or aim to achieve) an average room daylight factor of 2.5% and our design illuminance is 300Lux, then we may switch lights off at external illuminances exceeding 12kLux for some 3200 (around three quarters of) daylight hours.

Taken a step further one can approximate dimming controls for a specific case by also accumulating hour fractions (E/E' and $E < E'$) and also account for occupancy patterns and luminaire characteristics; thus supporting investment decisions regarding the installation of photoresponsive lighting control gear.

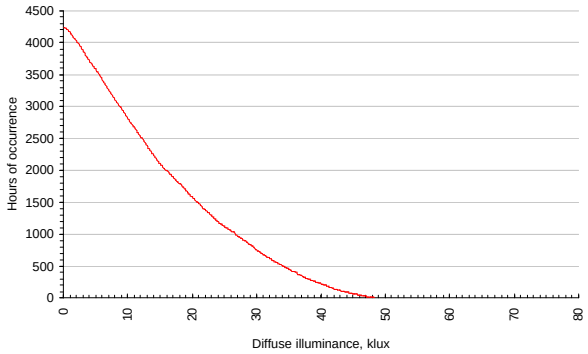

Figure 2 Daylight availability curve for Limburg

This process however is somewhat presumptuous: it assumes that a standard daylight factor expression is valid. This is not so for much of the year. Using [6] above, we can determine the percentage of the year during which the sky lies within a given clearness bin (from overcast (1) through to clear (8)) – Figure 3.

From this it is evident that sky conditions are strongly skewed towards the overcast end of the scale. However, the sky still exhibits a strong degree of anisotropy (non-uniform brightness distribution) for much of the year. During these times a standard daylight factor expression is **not** strictly valid – since it presupposes that the sky vault is overcast! For this reason increasing use is being made of more general daylighting prediction techniques. For example Robinson (2000) has developed a simple all-purpose analytical daylight model and sophisticated lighting simulation programs such as the backwards monte-carlo ray tracing program *Radiance* (Larson et al, 1998) can simulate daylighting under anisotropic skies and for scenes of arbitrary complexity.

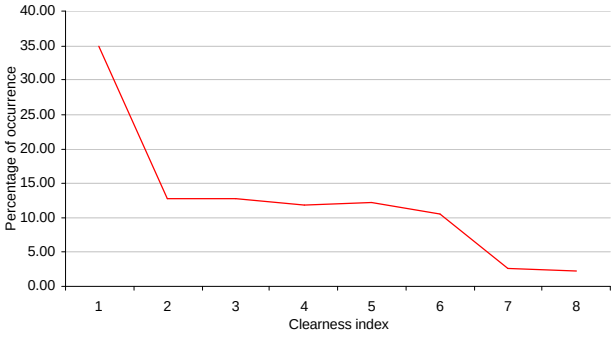

Figure 3 Sky clearness distribution for Limburg

Also related to daylight, one can plot a curve of daylight hours throughout the year (Figure 4). This can be achieved either by applying a corollary of [3] above (so that daylength d is $24\cos^{-1}\left(-\tan i \tan d\right)/p$ for each day, or perhaps more conveniently using an equation of the form;

$$d = \bar{d} + \tilde{d}\cos\left(2pj'/365\right) \quad \ldots[10]$$

in which $\bar{d}$ is the mean daylength (the mean of the two solstices) and $\tilde{d}$ is half the swing between the winter (w) and summer (s) solstices ($\tilde{d} = (d_w - d_s)/2$) and j' is $j+10$ to shift the cosine wave phase to coincide with the solstices. The sign of the daylength amplitude $\tilde{d}$ implicitly corrects for Northern (-) and Southern (+) hemispheres.

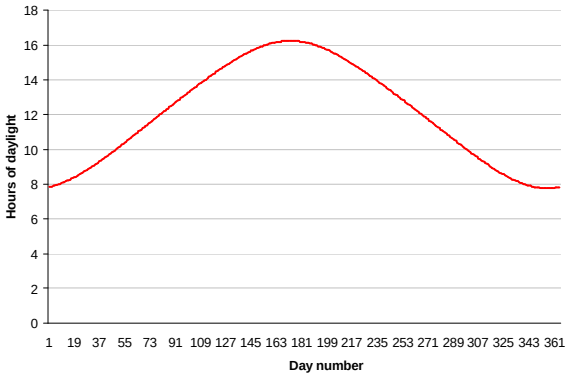

Figure 4 Daylengths throughout the year for Limburg

At high latitudes (say $|i| \geq\sim 60^o$) this can be helpful in evaluating the (de)merits of designing for large glazed areas when the daylighting and solar contributions during the course of the day are likely to be weak; so that the glazing gains loss ratio is small.

Irradiation surface plot

Building orientation, façade design and initial decisions regarding the use of active solar energy conversion systems can each be informed by irradiation surface plots. That is the variation of annual global solar irradiation (Whm^{-2}) over the range of receiving plane tilts (b) and orientations (a_w).

Determination of the beam (or direct normal) irradiance is relatively straightforward;

$$I_{bq} = \left(I_g - I_d\right)\cos q \,/ \sin g \qquad \ldots[11]$$

in which the cosine of the angle of incidence (q) is determined by the expression,

$$\cos q = \cos g \cos a' \sin b + \sin g \cos b \qquad \ldots[12]$$

and a' is the collector-solar azimuth ($a' = a - a_w - 2p$ for a - a_w > p , else $a' = a - a_w + 2p$). The determination of diffuse irradiance at the receiving plane from the sky vault follows from the well known Perez model (Perez 1990) which represents diffuse anisotropy due to circumsolar and zenith/horizon brightening:

$$I_{dq} = I_d\left(\begin{matrix}\left[1-F_1\right]\left[1+\cos b\,/\,2\right]+ \\ F_1 \cos q/\cos Z + F_2 \sin b\end{matrix}\right) \qquad \ldots[13]$$

where $F_{1,2}$ are circumsolar and horizon brightness coefficients from statistically derived coefficients f_{ij} ($F_1 = \max\left(0,\, f_{11} + f_{12}\Delta + f_{13}Z\right)$ and $F_2 = f_{21} + f_{22}\Delta + f_{23}Z$: see Table 1 for f_{ij}) based on sky clearness e and for equation stability the solar disc must not lie within a 5 degree arc of the zenith ($Z = p/2\text{-}g \geq 0.087$ radians). Sky clearness for this model has the form:

$$e = \frac{I_g / I_d + 5.535\cdot 10^{-6} Z^3}{1 + 5.535\cdot 10^{-6} Z^3} \qquad \ldots[14]$$

A final diffuse contribution to the ground I_{rgq} can be found as follows:

$$I_{rgq} = I_g r_g \left(1 - \cos b\right)/2 \qquad \ldots[15]$$

Accruing direct, sky and ground diffuse irradiances ($I_{gq} = I_{bq} + I_{dq} + I_{rgq}$) for the set of sunup hours for Limburg for 5 degree increments of collector tilt and orientation, we have an annual irradiation surface plot – Figure 5.

This chart in fact plots irradiation variance relative to the horizontal plane. Thus, the irradiation at a given azimuth and orientation is found by multiplying the global horizontal irradiation of 1.02 MWhm^{-2} by the mid-range of one of the above coloured bins, so that we have 1.2 MWhm^{-2} for a south facing collector tilted at 40^o from the horizontal plane.

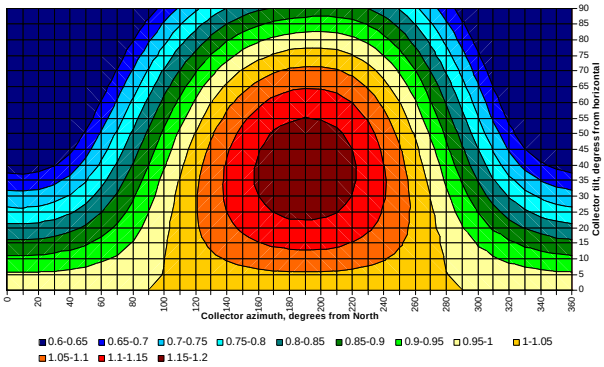

Figure 5 Solar availability surface plot for Limburg

Frequency distributions and monthly statistical summaries

The upper chart in Figure 6 shows solar radiation frequency distribution for each bin (red) as well as the cumulative distribution (blue), from which we can identify say the number of occurrences above or below some threshold. It is also useful to gain some appreciation of the time varying nature of solar radiation as well as the distribution of solar intensity. Figure 6 for example illustrates monthly minimum, maximum and upper and lower quartiles of global horizontal irradiance.

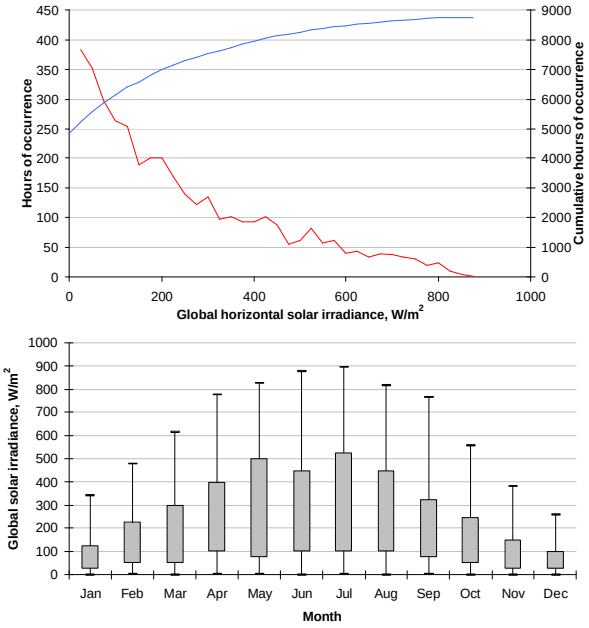

Figure 6 Solar radiation frequency (upper) and temporal (lower) distributions for Limburg

The mean, variance, standard deviation, skew and kurtosis of each climatic variable is also computed.

SYNOPTIC PARAMETERS

This family of climatological variables relates to temperature, humidity and wind. In processing the climate data under these categories, ClimPro produces a wind rose, predicts ground temperatures, plots data on a psychrometric chart and produces charts of temporal and frequency distributions.

Wind rose

ClimPro produces a wind rose (Figure 7) which has a similar definition to that which is presented within the European Wind Atlas (Troen and Petersen, 1989), but the segment size can be user defined (i.e. it can be other than 30°). Three sets of curves are created within these segments. The first of these (black curve) indicates the fraction of the year in which the wind has approached from the *i*th segment for which we accrue a *j*+1 count ($\sum d_j / \sum d_{ij}$). The second (red curve) plots the fraction of the cumulative wind speeds that approached from the *i*th segment ($\sum v_j / \sum v_{ij}$) and the third (blue curve) plots a representation of the fraction of cumulative kinetic energy flux within the *i*th segment ($\sum v_j^3 / \sum v_{ij}^3$). Each curve is normalised according to the maximum value that occurred in all segments. From this we have an a-priori view of the relative frequency with which winds approach from each direction, together with their strength. The box to the lower left of the rose contains respectively the percentages of direction, speed and energy within the dominant segment.

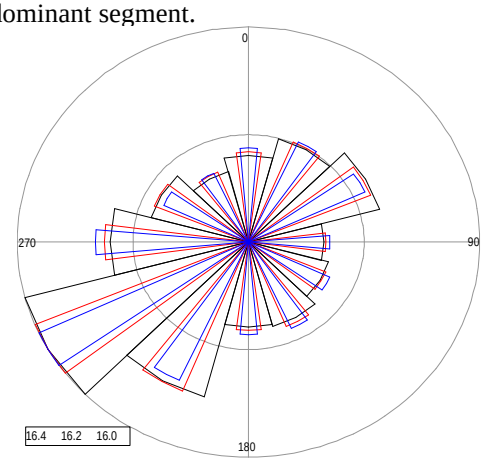

Figure 7 Wind rose for Eindhoven.

Unfortunately wind direction prediction within Meteonorm is poor as there is no stochastic perturbation, such that a single direction persists for a given month. One way around this is to create hourly wind directions given a wind direction probability distribution (which may have been published in tables or in the form of an alternate wind rose). Clearly it is not interesting simply to recreate a rose, but it may well be useful to create a more realistic hourly climate file for later use with a simulation program. Now, if we compose an array of *n* cumulative probabilities that the wind will approach from each segment moving clockwise from North, then we can deduce a wind direction *d* for the *j*th hour by cycling through the set of cumulative probabilities: (e.g. for $i = 1$ to n if $P_{i+1} > G_j \geq P_i$ then the direction d_j is $360i/n$, where G is a pseudo random number ($0 = G = 1$) for the *j*th hour). This is similar to the inverse function method of stochastic modelling, but for the simple case of a 1 by *n* state transition probability matrix. Figure 7 has been created on this basis using cumulative probabilities from the European Wind Atlas (1996).

Ground temperature

The temperature at the soil surface t_s can be found (approximately) using an expression similar to that in [10], so that for the *j*th day,

$$t_s = \bar{t} - \tilde{t}\cos(2p[j - j']/365) \qquad \ldots[16]$$

in which *j'* is a constant (the *j* day at which the minimum mean daily temperature occurred) to shift the cosine wave phase to ensure coincidence with the minima; $\bar{t}$ and $\tilde{t}$ are respectively the annual mean and swing in mean daily temperature. Now the decrement factor (the ratio of the amplitude at depth

d to that at the surface) f decays exponentially with depth from the surface and can be represented by,

$$f = \exp\left(-d\left[p/365a\right]^{1/2}\right) \quad \text{...[17]}$$

for a soil of thermal diffusivity a (m^2day^{-1} = 8.64 x $10^4 k/\rho C_p$). Furthermore, the temperature wave in the soil lags behind the surface wave due to the time taken to heat/cool the soil. This time lag ($days.m^{-1}$) is expressed by;

$$L = \frac{1}{2}\left(\frac{365}{pa}\right)^{1/2} \quad \text{…[18]}$$

Now, combining equations [17] and [18] with [16] we have an expression for estimating temperature at depth d below the ground for the jth day (based on that due to Labs, 1982);

$$t_d = \bar{t} - \tilde{t} f \cos\left(2p\left[j - j' - dL\right]/365\right) \quad \text{…[19]}$$

It is interesting to use this expression to explore the variation in ground temperature profile during the course of a year (Figure 8). As well as presenting further ground temperature relationships Labs (1982) provides a series of expressions for estimating the thermal contributions from this energy source and Athientis et al (2000) provide a means for estimating the temperature of air departing from a subterranean duct.

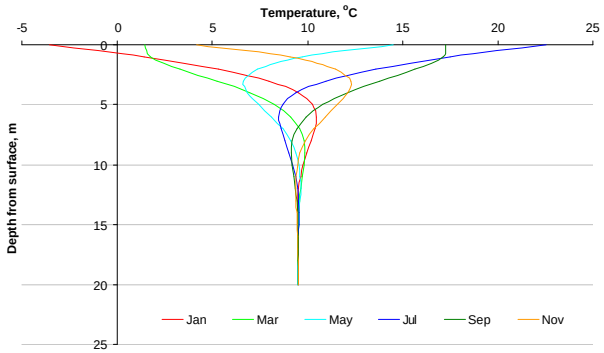

Figure 8 Ground temperature profiles for Limburg

Psychrometric chart

When plotted on a psychrometric chart, synoptic climate data reveals its psychrometric extremities from which one can formulate an a-priori view of the need for and potential of some form of evaporative cooling, or indeed for dehumidification. For this purpose we need only a relatively crude psychrometric chart. In common with the sunpath diagram and wind rose presented above, we can build this chart using an x,y scatterplot in which dry bulb temperature and moisture content (assuming constant humidity ratio) are the x,y co-ordinates.

In the first instance then, we should define a set of percentage saturation curves, say at 10% increments (10→100) throughout the temperature range -10 ≤ t ≤ 60°C at 1°C increments. Now, given a percentage saturation m and dry bulb temperature T (K) we can find the moisture content g using the expression;

$$g = mg_{ss}/100 \quad \text{…[20]}$$

in which the moisture content of a mixture of saturated vapour and air g_{ss} is;

$$g_{ss} = \frac{0.62197 f_s P_{ss}}{P - f_s P_{ss}} \quad \text{…[21]}$$

where f_s is an enhancement factor;

$$f_s \begin{cases} -7.3\cdot10^{-6}T + 1.0044, & t < 11 \\ 1.32\cdot10^{-5}T + 1.004205, & 11 \le t < 26 \\ 4.05\cdot10^{-5}T + 1.003497, & 26 \le t \le 60 \end{cases} \quad \text{…[22]}$$

P is the atmospheric pressure (typically the standard barometric pressure, 101.325kPa) and P_{ss} the saturation vapour pressure is,

$$\log_{10} P_{ss} = \begin{cases} 9.5381 - 2663.91T^{-1}, & T < 273.15 \\ 30.59051 - 8.2\log_{10} T + & \\ 2.484\cdot10^{3}T - 3142.31T^{-1}, & T > 273.15 \end{cases} \quad \text{…[23]}$$

In the second of the two expressions above, T refers to the triple point of water ($T = t + 273.16$).

Moisture content and dry bulb temperature are simply represented by straight lines that continue either to the boundaries of the chart or until the saturation curve is intersected (saturation temperature is found iteratively and convergence is based, say for moisture content, on finding the temperature at which air at 100% saturation approximately equals the g of interest). All that remains then is to define the wet bulb temperature lines. To do this we use the so called 'psychrometric equation' for deriving the partial pressure of water vapour in an air-water vapour mixture P_s:

$$P_s = P'_{ss} - PA\left(t - t'\right) \quad \text{…[24]}$$

in which primed values refer to the wet bulb temperature (e.g. P'_{ss} is found [23] using the wet bulb temperature) and A (K^{-1}) is a constant depending on the method of measuring the wet bulb temperature (e.g. for aspirated (sling) psychrometers A = 6.66 x 10^{-4} for t ≥ 0, else A = 5.94 x 10^{-4}). The corresponding moisture content is then found by inserting P_s into [21], since at the wet bulb temperature the air is super-saturated in the vicinity of the thermometer's wetted gauze. With these four curve sets defined, we have a psychrometric chart (Figure 10).

Finally, to make use of this chart we must plot the climate data which simply requires that we derive

moisture content from dry bulb temperature and relative humidity. For this we can again make use of the psychrometric equation to find g given the wet bulb temperature. However, since both t' and P'_{ss} are unknown we must use another root finding algorithm which, by varying t', yields a solution when the difference between the given relative humidity f and that defined by [25] passes some convergence test,

$$f = 100 P_s / P_{ss} \qquad \ldots[25]$$

in which we use [23] and [24] for P_{ss} and P_s respectively. The corresponding wet bulb temperature is then used to find g using the above procedure. For a more complete description of psychrometry refer to Jones (1994).

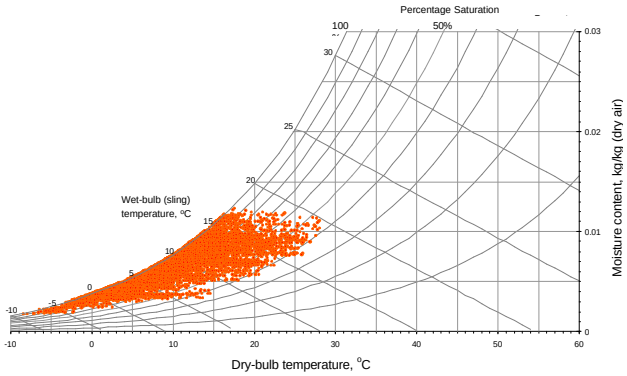

Figure 9 Hourly synoptic data for Limburg plotted on a psychrometric chart

Frequency distributions and monthly statistical summaries

Likewise with solar radiation, it is useful to express the frequency and temporal distributions of temperature, wind and humidity (Figures 10 to 13).

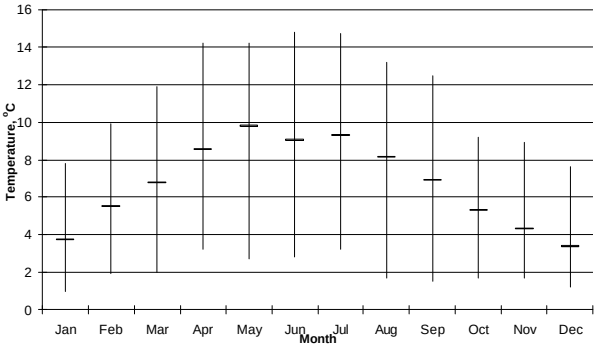

Figure 10 Monthly minimum, mean and maximum nocturnal temperature swings for Limburg

Figure 10 for example illustrates the potential for nocturnal convective cooling to alleviate summertime overheating risk – which itself can be judged on the basis of the temperature distributions given in Figure 11. Figure 12 indicates not only the potential for natural ventilation but also of the distribution of winds throughout the year as a means for renewable energy generation. Finally, Figure 13 inidcates the potential for evaporative cooling (if any) and the need for or otherwise of active (de)humidification.

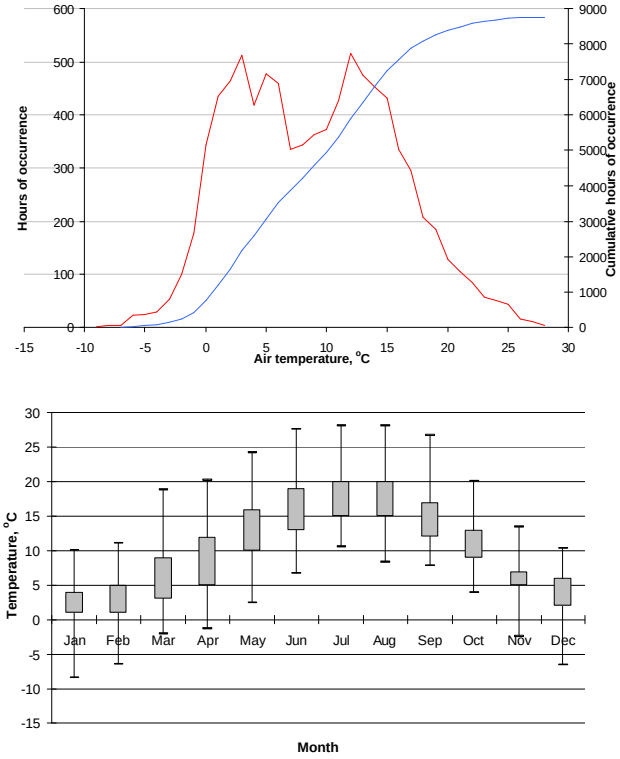

Figure 11 Temperature frequency (upper) and temporal (lower) distributions for Limburg

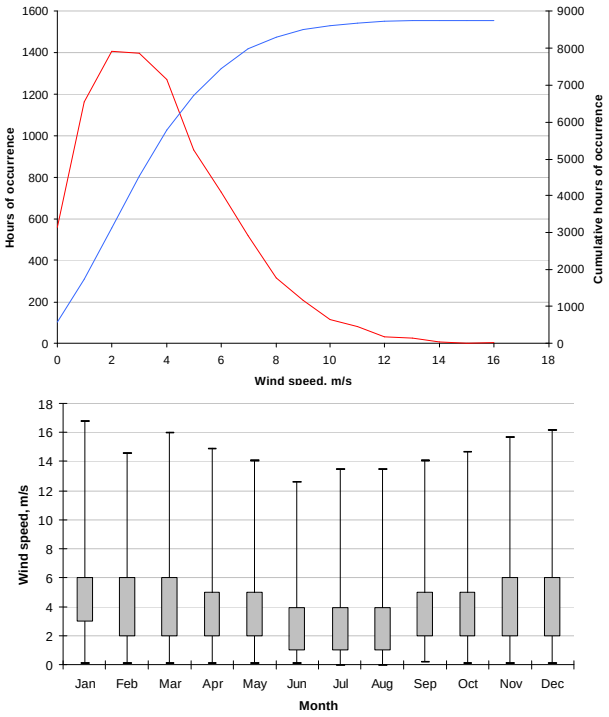

Figure 12 Wind frequency (upper) and temporal (lower) distributions for Limburg

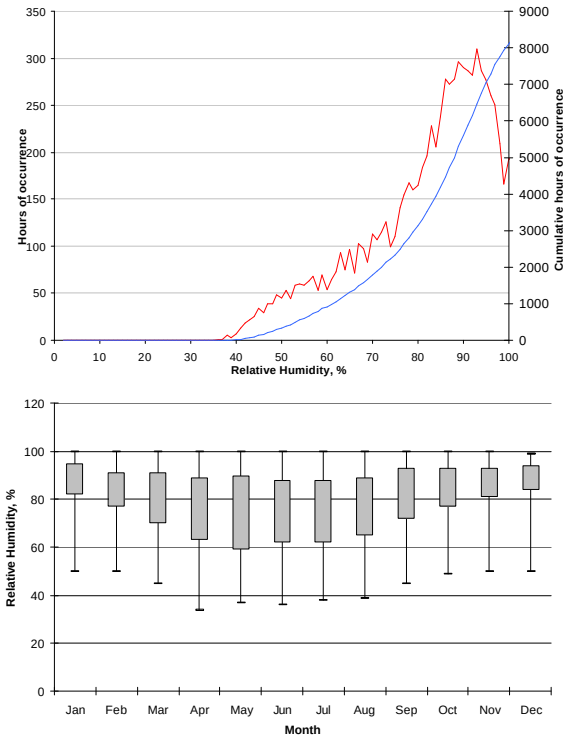

Figure 13 Relative humidity frequency (upper) and temporal (lower) distributions for Limburg

In addition to these charts, ClimPro derives heating and cooling degree days (e.g. for a year of *j* days heating degree days, $DD = \sum t' - \bar{t}_j \quad (\bar{t}_j < t')$, for a given base temperature *t'*). For Limburg and using this climate file, the heating (15.5°C base) and cooling (18°C base) degree days are 2531 and 14 respectively.

CONCLUSIONS

With a reasonably modest amount of programming, a relatively mundane and difficult to interpret climate data file can be transformed in just a few seconds into a series of useful graphical design aids to stimulate thinking during the very early stages of concept environmental design.

Some internal assumptions are made in processing the climate, such as soil thermal diffusivity for the ground temperature profiles and ground reflectance for the irradiation surface plot. A future version of the climate processing tool might usefully include the ability to define additional inputs as well as access to defaults. This might include for example the ability to define an illuminance datum and daylighting factor for analysis of photoresponsive dimming using the daylight availability model or a procedure for testing the effectiveness of some form of evaporative cooling using the psychrometric equations and associated chart. Another useful feature might be the ability to control the software to process between particular dates and/or times of day. Finally, it would be useful to incorporate an evapotranspiration model to help inform rainwater harvesting strategies.

REFERENCES

Athientis, A.K., Santamouris, M., Kyprianou, A., *Application of ground cooling/heating for HVAC air precooling/preheating*, Proc. PLEA 2000, Cambridge UK, James and James, p94-99, 2000.

British Standards Institution, *Code of practice for daylighting*, BS 8206: Part 2, 1992.

Jones, W.P., *A review of CIBSE pychrometry*, Building Services Engineering Research and Technology, 15(4), p189-198, 1994.

Labs, K., *Regional analysis of ground and above ground climate conclusion*, Underground Space, vol. 7 p37-65, 1982.

Perez, R., Ineichen, P., Seals, R., *Modelling daylight availability and irradiance components from direct and global irradiance*, Solar Energy 44(5) p271-289, 1990.

Robinson, D., Baker, N.V., *Simplified Modelling: recent developments in the LT Method*, Building Performance 3(1), p14-19, 2000.

Spencer, J.W., *Fourier series representation of the position of the sun*, Search 2(5) p172, 1971.

Troen, G.W., Petersen, E.L., *European Wind Atlas*, Commission of the European Communities, 1989.

ε bin	A_1	A_2	A_3	A_4	f_{11}	f_{12}	f_{13}	f_{21}	f_{22}	f_{23}
1 (1.000 ≤ ε < 1.065)	97.24	-0.46	12.00	-8.91	-0.008	0.588	-0.062	-0.060	0.072	-0.022
2 (1.065 ≤ ε < 1.230)	107.22	1015	0.59	-3.95	0.130	0.683	-0.151	-0.019	0.066	-0.029
3 (1.230 ≤ ε < 1.500)	104.97	2.96	-5.53	-8.77	0.330	0.487	-0.221	0.055	-0.064	-0.026
4 (1.500 ≤ ε < 1.950)	102.39	5.59	-13.95	-13.90	0.568	0.187	-0.295	0.109	-0.152	-0.014
5 (1.950 ≤ ε < 2.800)	100.71	5.94	-22.75	-23.74	0.873	-0.392	-0.362	0.226	-0.462	0.001
6 (2.800 ≤ ε < 4.500)	106.42	3.83	-36.15	-28.83	1.132	-1.237	-0.412	0.288	-0.823	0.056
7 (4.500 ≤ ε < 6.200)	141.88	1.90	-53.24	-14.03	1.060	-1.600	-0.359	0.264	-1.127	0.131
8 (6.200 ≤ ε)	152.23	0.35	-45.27	-7.98	0.678	-0.327	-0.250	0.156	-1.377	0.251

Table 1 Coefficients for the Perez diffuse luminous efficacy and irradiance models